



ELSEVIER

Contents lists available at ScienceDirect

Engineering Applications of Artificial Intelligence

journal homepage: www.elsevier.com/locate/engappai

Change detection in SAR images by artificial immune multi-objective clustering

Ronghua Shang^{a,*}, Liping Qi^a, Licheng Jiao^a, Rustam Stolkin^b, Yangyang Li^a^a Key Laboratory of Intelligent Perception and Image Understanding of Ministry of Education of China, Xidian University, Xi'an, China^b School of Computer Science, University of Birmingham, Edgbaston, Birmingham B15 2TT, UK

ARTICLE INFO

Available online 25 February 2014

Keywords:

Synthetic Aperture Radar (SAR)
Image change detection
Artificial immune system
Multi-objective optimization (MO)

ABSTRACT

This paper addresses the problem of unsupervised change detection in Synthetic Aperture Radar (SAR) images. Previous approaches have used evolutionary clustering optimization methods, which can suffer from reduced accuracy, because they often use only a single objective function and can easily become trapped at locally optimal values. To overcome these difficulties, we propose a new approach which combines the artificial immune system (AIS) theory with a multi-objective optimization algorithm. First, the self-adaptive artificial immune multi-objective algorithm is adopted to pre-sort the difference image. During this procedure, the difference image is categorized into three classes – changed class, unchanged class and uncertain samples. Second, based on wavelet decomposition to extract features from the difference image, the immune clonal multi-objective clustering algorithm is used to search for the optimal clustering centers of uncertain samples, labeling them as changed or unchanged. Experimental comparisons with four state-of-the-art approaches show that the proposed algorithm can obtain a higher accuracy, is more robust to noise, and finds solutions which are more globally optimal. Additionally, the proposed algorithm can improve the local search ability for the optimal solutions and produces better cluster centers.

© 2014 Elsevier Ltd. All rights reserved.

1. Introduction

Change detection in remote sensing, is a process that analyzes images of the same geographical area at different times in order to identify any changes which have taken place between the two assigned acquisition dates (Celik, 2009). Over the past three decades, there have been significant developments in both the remote imaging devices and also the methods for detecting changes in the images (Gong et al., 2012). Being insensitive to atmospheric and illumination conditions, the Synthetic Aperture Radar (SAR) system has the advantages of being an all-day, all-weather device, as well as offering wide area coverage (Curlander and McDonough, 1991). Therefore SAR images are considered to be more useful than other remote sensing methods for detecting change over significant geographical areas. However, SAR images suffer from speckle noise, making change detection in SAR images more challenging than in conventional optical images (Zhang et al., 2013).

This paper introduces a novel approach to change detection in SAR images, which makes use of multi-objective artificial immune

system (AIS) methods to optimally cluster image pixels into changed or unchanged classifications. Our method comprises two main novel contributions.

- (1) Previous literature has shown the benefits of Evolutionary Algorithms (EA) (Droste et al., 2002) or genetic algorithms (GA) (Goldberg and Holland, 1988) for numerical optimization of the parameters of clustering or statistical models of changed and unchanged pixels, which can then be used for pixel categorization. However, pre-dominantly, these methods rely on optimizing with respect to a single objective-function, which makes them vulnerable to convergence on locally optimal solutions, reducing their accuracy. In contrast, this paper shows how to incorporate multi-objective optimization within an AIS approach, and demonstrates superior accuracy of change detection over the single-objective approaches.
- (2) The methods described in previous literature apply sophisticated modern optimization methods; however, pre-dominantly, these only make use of simple gray-level values of difference-image pixels. This single feature alone means that such methods do not fully exploit all of the information available in the difference image. Furthermore, SAR images are particularly vulnerable to speckle-noise, which cannot be

* Corresponding author. Tel.: +86 02988202279.

E-mail address: rhshang@mail.xidian.edu.cn (R. Shang).

overcome by using individual pixel features, requiring additional contextual information. In contrast, our method shows how different kinds of features can be combined within the pixel classification optimization process. Apart from pixel gray levels, our method also exploits wavelet texture features. This enables us to successfully overcome severe speckle noise, and demonstrate superior change detection performance over single feature methods.

In order to combine the benefits of these two different kinds of features, we propose a two-stage procedure for change detection. In the first stage, pixel gray levels alone are used to perform an initial segmentation. Those pixels, for which gray levels provide enough information for high confidence, are categorized into “changed” and “unchanged” classes. Any remaining pixels are categorized as “uncertain”. The second stage uses additional texture features, based on wavelet transforms, to provide the additional information needed to classify these uncertain pixels.

The reason for the two stage process is that this saves computational expense (compared to combining both features in a single stage, or reversing the order of the stages). The proposed two-stage procedure means that the maximum number of pixels are classified using only the simplest and cheapest features. The more complex and expensive features are then used to classify any remaining pixels. In contrast, if both features were fused into a single stage, then the system would suffer additional expense due to informational redundancy. Furthermore, it is not obvious how to best combine these two different features in order to carry out single image segmentation.

This paper is organized into five sections. Section 2 provides a review of SAR change detection methods, evolutionary algorithms and artificial immune systems, and highlights the contributions of this work by placing it in context. Section 3 introduces the multi-objective model and related definitions, and describes the steps of the proposed method in detail. Section 4 presents the experimental results and analysis. Section 5 provides a summary and conclusions.

2. Related work

In previous literature, several methods for SAR image change detection have been proposed. Some are supervised and others are unsupervised (Belghith et al., 2013). Supervised approaches rely on the methods of supervised classification to detect changed and unchanged regions; however this process requires ground truth data in order to extract a suitable training set for the learning process of the classifiers. For many real applications, suitable ground truth training data is not available and would be prohibitively difficult to obtain. In contrast, unsupervised classifiers do not require any training data, and so unsupervised change detection approaches can be more useful in many SAR change detection applications (Ghosh et al., 2011). This paper focuses on the problem of unsupervised change detection.

Unsupervised change detection methods are typically posed in terms of a two-class discrimination problem, applied to a difference image derived from the two original SAR images from two acquisition dates. These unsupervised change detection methods can generally be divided into three steps: (1) image pre-processing, (2) difference image calculating, and (3) classification of the difference image. In the third step, several unsupervised classification methods have been proposed, such as the Expectation Maximization (EM) method (Amayr and Bouguila, 2013), Markov Random Field (MRF) (Ghosh et al., 2013), the Gaussian mixture model (GMM) (Zhang et al., 2013), *K*-means (Celik, 2009), Fuzzy C-means (FCM) (Dunn, 1973), Images fusion and fuzzy clustering (Gong et al., 2012) etc. EM (Dempster et al., 1977) and MRF (Geman and Geman, 1984; Besag, 1986) methods are based on the Bayes

theory. The EM based method is free of parameters and selects the decision threshold for identifying changed and unchanged regions while minimizing the overall change detection error with the grayscale pixel values of the difference image. EM based methods need to set the value of initial parameters, and this in turn influences the accuracy of the threshold. The MRF based and GMM based approaches depend on reliable estimation of parameters which influence the spatial contextual information during the change detection process, and also on a priori assumptions in modeling the difference image data which influence the accuracy of the change detection result. *K*-means and FCM methods are two well-known classification techniques which perform well on many problems. However they suffer from accuracy problems in detecting changed areas under strong noise contamination of images (common in SAR images which suffer from speckle noise). Their performance is also dependent on the number of the classes.

To address the above problems, GA based methods have been proposed and used to improve automatic parameter estimation or to avoid the need for parameter estimation, a priori assumptions or pre-setting the number of classes. Bazi et al. (2009) used the EM algorithm initialized with a robust strategy based on genetic algorithms to estimate the statistical parameters of the changed and unchanged classes, which are assumed to follow a generalized Gaussian distribution in the analyzed log-ratio image. Celik (2010a) adopted an *N* components Gaussian mixture model (GMM) and a genetic algorithm to achieve image change detection by using the GA to estimate the parameters of the GMM. These two methods use genetic algorithms to estimate statistical parameters, thereby reducing errors due to poor parameter estimates and increasing the automation of change detection over methods where parameters are selected by hand. Furthermore, Celik (2010b) proposed another change detection method which uses a GA method to find the final change detection mask with minimum cost, by evolving the initial realization of the binary change detection mask through generations. This method can produce the change detection result without needing a priori assumptions, such as pre-setting the number of classes.

GA based methods also have some disadvantages in handling individual solutions within a population. The randomness of crossover and mutation operators means that GA based methods sometimes fail to reproduce excellent individuals, which can increase the number of iterations needed to reach an optimal solution. In contrast, the clone operator which is included in artificial immune algorithms maintains good affinity antibodies and increases the probability of selecting good antibodies. Artificial immune systems (AIS) also imitate other biological immune functions, providing features such as protective immunity, immune memory, immune learning (Yang et al., 2011), etc. Artificial immune algorithms have previously been successfully applied to solving complex problems in image processing (Yang et al., 2011), pattern classification (Aydin et al., 2010) and other applications (e.g. Chang et al., 2009; Kalinli and Karaboga, 2005).

Therefore, in this paper, we adopt an AIS method and show how it can be used to successfully classify difference images for SAR image change detection. Benefits of the proposed approach are self-adaptive and retention of good affinity antibodies, without the need for a priori knowledge such as number of categories, training data or parameter models.

AIS based methods can broadly be divided into single objective and multi-objective optimization methods. As regards single objective optimization methods, literature variety of AIS methods have been proposed, and shown to outperform GA methods in several applications. Timmis et al. (1999) presented a resource limited artificial immune network model which was applied to solving unsupervised classification problems with complex iris data. Huang and Jiao (2008) presented an immune clonal clustering method by combining artificial immune networks and support vector machines for SAR image segmentation. Based on the work

of Celik (2010b), Wan and Jiao (2011) proposed a method of using a clonal selection algorithm, instead of genetic algorithm, to improve the accuracy of change detection results. Li et al. (2011) proposed a quantum-inspired immune clonal algorithm, based on the grayscale pixel values of the difference image, to search for optimal clustering centers for change detection.

All of the above algorithms are essentially single objective optimization methods which are based on artificial immune algorithms. However, despite often outperforming GA methods, these methods also have some problems in practical applications. SAR images are prone to speckle noise, which can be difficult to model, and this can lead to single objective change detection methods converging on unilateral optimal solutions which fail to take account of global performance, leading to suboptimal cluster centers or solutions. In contrast, the multi-objective optimization algorithm can enlarge the search space and improve the diversity of solutions.

A variety of multi-objective artificial immune systems (Omkar et al., 2008) have been proposed since the first pioneering study on evolutionary multi-objective algorithms was published in 1985 (Schaffer, 1985). The first work using AIS for evolutionary multi-objective optimization was described in (Yoo and Hajela, 1999). Later work, Cutello et al. (2005), proposed a modified method of Pareto archived evolution strategy algorithms, using a polypeptide chain and two immune operators. Coello and Cortes (2002) first proposed a clonal selection principal for multi-objective optimization algorithm. Bandyopadhyay et al. (2007) proposed multi-objective genetic clustering for pixel classification in remote sensing imagery. Yang et al. (2011) proposed a SAR image segmentation approach which uses an artificial immune multi-objective algorithm with fused complementary features. Zou et al. (2013) proposed a method of multi-objective optimization using a teaching-learning-based optimization algorithm. These methods help enlarge the search space, generate a set of good solutions and improve the diversity of solutions.

A drawback of previous multi-objective AIS methods is that they pre-dominantly use only a single kind of image feature which is the grayscale pixel values. However, SAR images contain many other kinds of information, such as grayscale pixel values, texture, spatial features and other kinds of features. Therefore, one feature alone cannot utilize all information contained in a SAR image, and it would be advantageous to develop new approaches which utilize more of the available information.

The key contribution of this paper is that we use both grayscale pixel values and texture features of the difference image and propose a novel unsupervised method which combines artificial immune system with multi-objective optimization for SAR image change detection. This procedure consists of two stages, which both use multi-objective AIS in different ways.

- (1) In the first stage, a self-adaptive artificial immune multi-objective algorithm is used to pre-sort the difference image into three classes (changed class, unchanged class and uncertain samples), based on difference image gray-level pixel values alone.
- (2) The second stage uses additional features to classify any pixels identified as “uncertain” during the first stage. A non-subsampled wavelet transform is applied to the difference image, yielding a 10 dimensional texture feature vector for each pixel. An immune clonal multi-objective clustering algorithm is then used to optimally separate these 10D vectors into two clusters, representing the changed and unchanged classification.

3. Artificial immune multi-objective clustering algorithm

This section introduces the multi-objective models and related definitions, describes the mathematical details of each of the two

stages of our change detection method, and provides an overall summary of the change detection procedure.

3.1. Multi-objective optimization model and related definitions

Multi-objective optimization problems (Deb, 2001) can be described as

$$\begin{aligned} \min \mathbf{y} = \mathbf{f}(\mathbf{x}) &= (f_1(\mathbf{x}), f_2(\mathbf{x}), \dots, f_n(\mathbf{x}))^T \\ \text{s.t. } g_i(\mathbf{x}) &\leq 0 \quad i = 1, 2, \dots, q \\ h_j(\mathbf{x}) &= 0 \quad j = 1, 2, \dots, p \end{aligned} \quad (1)$$

where $\mathbf{x} = (x_1, \dots, x_n) \in \mathbf{X} \subset R^n$ represents the n -dimensional decision vector, \mathbf{X} is an n -dimensional decision space, $\mathbf{y} = (y_1, \dots, y_n) \in \mathbf{Y} \subset R^n$ represents the n -dimensional target vector, and \mathbf{Y} is an m -dimensional objective space. The objective function $\mathbf{f}(\mathbf{x})$ denotes n mapping functions from the decision space to the objective space. $g_i(\mathbf{x}) \leq 0$ ($i = 1, \dots, q$) represents q inequality constraints and $h_j(\mathbf{x}) = 0$ ($j = 1, \dots, p$) defines p equality constraints.

The proposed multi-objective SAR image change detection model has two objectives. Its model can therefore be described as

$$\min \mathbf{F}(\mathbf{x}) = (f_1(\mathbf{x}), f_2(\mathbf{x}))^T \quad (2)$$

where $\mathbf{x} = (x_1, \dots, x_m)$ represents the m -dimensional features constituting a decision vector. The objective function $\mathbf{F}(\mathbf{x})$ defines two mapping functions from the decision space to the objective space. These two functions are conflicted with each other and cannot be optimized simultaneously. Thus, there is no unique global optimal solution and a multi-objective optimization algorithm can generate a set of non-dominated solutions.

We now present some basic concepts of AIS-based multi-objective optimization methods. A searching problem can be regarded as an antigen in AIS. The multi-objective optimization defined by Eq. (1) can be seen as the antigen. The candidate solutions of Eq. (1) are called antibodies. The binding intensity between antigen and antibody is named the antigen-antibody affinity, which are the values of objective functions of candidate solutions.

The concept of dominance in multi-objective optimization is described here. For antibodies $\mathbf{x}, \mathbf{x}^* \in \mathbf{X}$, \mathbf{x}^* is called Pareto-dominance (Deb, 2001) and recorded as $\mathbf{x}^* \text{mac}; sc; \mathbf{x}$ when \mathbf{x}^* satisfies

$$(\forall i \in \{1, \dots, n\} : f_i(\mathbf{x}^*) \leq f_i(\mathbf{x})) \wedge (\exists j \in \{1, \dots, n\} : f_j(\mathbf{x}^*) < f_j(\mathbf{x})) \quad (3)$$

An antibody \mathbf{x}^* is said to be non-dominated if \mathbf{x}^* meets the following rule (Deb, 2001):

$$\neg \exists \mathbf{x} \in \mathbf{X} : \mathbf{x} > \mathbf{x}^* \quad (4)$$

In this paper, the procedure of the proposed method has two steps, each of which uses a multi-objective method. In each of these two steps, we adopt different sets of objective functions. The first step uses grayscale pixel values to initialize the population, and each antibody of the population represents one possible classification result. The first step searches for detection results which have the nearest neighbor relationship between the intra-class samples and have the smallest distance between the samples and the clustering centers of the intra-classes. So in this step, the adaptive classification problem is changed into two objective functions, and the multi-objective model can be described as

$$\mathbf{F}(\mathbf{x}) = (\text{Dev}(\mathbf{x}), \text{Conn}(\mathbf{x}))^T. \quad (5)$$

The details of functions Dev and Conn will be described in Section 3.2.2.

The second step uses the texture information of SAR images to initialize a population, where each antibody of population represents a possible set of clustering centers for uncertain samples.

The second step searches for a set of clustering centers which assign the best possible classifications to samples labeled as uncertain in the first stage. Such optimal classifications should produce the smallest possible differences between the intra-class samples and the largest possible differences between the inter-classes samples. Again, these two competing requirements can be written as a multi-objective model and can be described as

$$F(\mathbf{x}) = (JM(\mathbf{x}), XB(\mathbf{x}))^T, \quad (6)$$

where the details of the functions JM and XB will be described in Section 3.3.3.

The two stages, described above, make use of different sets of objective functions. We now explain the reasons for this.

Firstly, the initialization requirements for each stage are different. In the first stage, in order to fully automate the algorithm, it adopts the neighbor relationship based antibody link mechanism to initialize the population. This encoding mechanism does not require hand initialization of the number of classes. It uses the neighbor relationship to classify the difference image and generate the number of categories. For good results, objective functions require the obtained number of categories to control the relationships between inter-classes. If the number of categories is not taken into account, then an extreme case can arise wherein the number of categories becomes equal to the number of samples, and each sample forms its own cluster center, contrary to the original purpose of the data classification. In contrast, the second stage initializes cluster centers randomly, using a pre-known number of categories (two categories, changed and unchanged). So the objective functions of the second stage do not need the number of categories to control the relationship between inter-classes.

Secondly, in the first stage, the population of antibodies represents a set of possible results for change detection. This uses an antibody link mechanism based on neighbor relationships. For good results, these objective functions need to measure the neighborhood relationship between each component of one antibody. In contrast, in the second stage, each antibody only has two components (the first one is the clustering center of the first category and the second one is the clustering center of the second category) and it does not need to measure the neighborhood relationship between each component of each antibody.

Thirdly, using different sets of objective functions in the first and second stages can increase the number of objective functions, enlarge the search space and improve the diversity of solutions.

3.2. Stage 1: initial clustering by gray-level using self-adaptive artificial immune multi-objective optimization

This section describes the first stage of our change detection method. In this stage, a self-adaptive artificial immune multi-objective optimization algorithm is used with gray-level pixel values of the difference image. This algorithm divides the difference image into three classes: changed, unchanged, and uncertain.

3.2.1. Initialization

We begin initialization by using the watershed transformation (Beucher, 1992) to partition the difference image into non-overlapping and homogeneous regions. Then, the number of these regions is used as the length of antibodies and the neighbor relationship based antibody link mechanism (Handl and Knowles, 2007) is used to initialize the population. This encoding mechanism can automatically determine the correct number of categories and is explained in Fig. 1. To illustrate this method, Fig. 1 shows an example, where there are 10 components in an antibody \mathbf{p} , i.e., in this example, the watershed transformation partitioned the difference image into 10 regions. The components of the antibody are randomly selected integers from 1 to the length of the antibody.

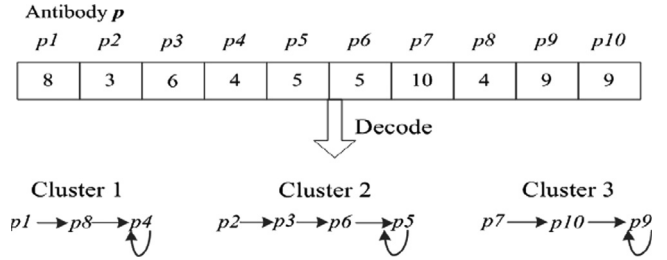


Fig. 1. The antibody encoding mechanism.

At the first iteration, $t = 0$, the population is initialized according to the above encoding mechanism and generates antibody groups with scale $x - \mathbf{P}(t) = [p_1(t), p_2(t), \dots, p_x(t)]^T$.

According to the above encoding mechanism, these antibodies will be divided into different categories by the neighbor relationship. However, the population is initialized with some randomness, and each antibody will have different neighbor relationships, so that each antibody may be divided into different classes. For example, in Fig. 1, this antibody \mathbf{p} is divided into three classes. It can be seen from Fig. 1 that p_1 is assigned number 8 randomly, where 8 represents the eighth element p_8 . p_8 is assigned number 4 randomly, where 4 represents the fourth element p_4 itself. Therefore, p_1 , p_4 and p_8 are in the same category. In the same manner, p_2 , p_3 , p_6 and p_5 are in the same category, and p_7 , p_{10} and p_9 are in the same category. Therefore, in this step, we will select some antibodies as the candidate solutions which have the same number of categories for the next step. The rule of selection is (1) record the number of categories of each antibody of population as A; (2) count the maximum number of antibodies, which have the same number A as each other and record this number as B; (3) select the antibodies which have the number B. These antibodies will be regarded as candidate solutions for the next step.

3.2.2. Affinity

Affinity (Yang et al., 2014) is defined in terms of the objective functions Dev and Conn of Eq. (5). For each antibody, these are defined as

$$f_1(\mathbf{p}_n(t)) = \text{Dev} = M(\mathbf{p}_n(t)) \times \sum_{i=1, c_i \in c_j \in c_i}^{M(\mathbf{p}_n(t))} d(p_{nj}, m_i), \quad m_i = \frac{1}{|c_i|} \sum_{p_{nj} \in c_i} p_{nj}(t). \quad (7)$$

$$f_2(\mathbf{p}_n(t)) = \text{Conn} = \begin{cases} \sum_{i=1}^s \sum_{j=1}^L \frac{d(p_{ni}(t), p_{nj}(t))}{j}, & p_{ni}(t) \in c_m \wedge p_{nj}(t) \in c_m \\ 0, & \text{otherwise} \end{cases} \quad (8)$$

where $M(\mathbf{p}_n(t))$ is the number of categories for antibody $\mathbf{p}_n(t)$ at the t -th iteration and is necessary for normalization, i.e., $M(\mathbf{p}_n(t)) \in [0, 1]$. c_i and c_m are the classification subsets. $p_{ni}(t)$ and $p_{nj}(t)$ are components in an antibody. m_i is the cluster center of subset c_i . s is the total number of components in an antibody. $d(p_{ni}(t), p_{nj}(t))$ is the Euclidean distances between the component p_{ni} and its L nearest neighbor components p_{nj} at the t -th iteration. j is a penalty factor. The greater the distance between the sample and its L -th neighbor is, the greater the penalty j . The minimum value of j , corresponding to no penalty, is 1. This strategy ensures that samples which are close to each other (most likely to be nearest neighbors according to the Euclidian distance) are most likely to be classified as the same class. The rule of neighborhood relations is shown in Fig. 2. Here we use the same example of antibody \mathbf{p} , as shown in Fig. 1, to explain the rule of neighborhood relations. First, we use the Euclidean distance to calculate the

neighbor relationship matrix D of antibody p , thus each component of antibody p has a distance vector with other components. Second, we arrange the components of distance vector in ascending order, and the L smaller components are the nearest neighbors of the component of antibody p . It can be seen from Fig. 2 that, for element $p1$ in antibody p , there are four nearest neighbors $p9$, $p10$, $p3$ and $p7$, among which $p9$ is the nearest one and $p7$ is the farthest one. So for $p9$, $j=1$; for $p10$, $j=2$; for $p3$, $j=3$, and for $p7$, $j=4$.

Eq. (7), describes the sum of the distances between all samples and the clustering centers. The smaller the value of this index, the more likely the classification of samples is to be correct. If this index does not consider the number of categories of samples, then extreme case can occur, where all samples form their own cluster centers, so that the value of this index is zero, thus failing to satisfy the intended purpose of classification. Therefore, in order to avoid this extreme case, the choice of number of categories is very important. Eq. (8) describes the relationship between samples. Nearest neighbor samples which have a greater probability of mutual consistency will be labeled as belonging to the same class. It is helpful to ensure that samples in the same class have the nearest neighbor relationship. Therefore, these two objective functions are mutually complementary. They seek an optimal image segmentation wherein the distance between each sample and its respective cluster center is minimized, and the samples of the same class occur in close proximity to each other. However, Eqs. (7) and (8) are also mutually exclusive. The minimum value of Eq. (8) means that the samples are close to each other, which will increase the sum of the distances between all samples and the clustering centers. The minimum value of Eq. (8) means that all the samples are near their clustering centers, which will increase the value of Eq. (7). Therefore, it is generally difficult to find minimum solutions of Eqs. (7) and (8) and simultaneously, and so a set of non-dominated solutions is obtained.

3.2.3. Selection operator

The selection operator is used to select the best antibodies from the previous iteration, to form a new antibody population which increases local affinity. This process divides antibodies into non-dominated or dominated antibodies and selects non-dominated antibodies for the new population. To search for non-dominated antibodies, an antibody p^* ($p^* \in P$) is a non-dominated antibody, if and only if the following conditions are satisfied:

$$\neg \exists p \neq p^* \in P, (f_1(p^*) \geq f_1(p) \& f_2(p^*) > f_2(p)) \vee (f_1(p^*) > f_1(p) \& f_2(p^*) \geq f_2(p)). \tag{9}$$

Here the scale of the non-dominated antibodies is defined as S . If the number of non-dominated antibodies selected by this

operation is less than S , then non-dominated antibodies continue to be selected (random selection with replacement) until the scale S is reached. If the number of non-dominated antibodies is more than S , S non-dominated antibodies are selected randomly.

3.2.4. Clone operator

The clone operator is used to copy good affinity antibodies. The cloning rule at each iteration can be expressed as

$$\text{Num}(w) = P_c \times \frac{W}{S} \tag{10}$$

where w represents the number of non-dominated antibodies selected at each iteration. S is the scale of the non-dominated antibodies and P_c is the scale of the clone pool.

3.2.5. Immune operators

The immune operators include a crossover operator and a mutation operator which increase the diversity of the population, promote cooperation among antibodies and accelerate convergence rates. In this work, we use uniform crossover (Handl and Knowles, 2007) as crossover operator. This operator is explained in Fig. 3.

We also use the neighbor-based mutation operator (Handl and Knowles, 2007) which is defined in Algorithm 1.

Algorithm 1. The neighbor-based mutation operator

Preparation: The current population set $P = (p_1, p_2, \dots, p_n)$, the mutation rate p_m , the number of the nearest neighbors L .

Step1: $[POP, N_{um}] = \text{decode}(P)$, N_{um} is the number of categories for each antibody.

Step2: $[n, m] = \text{size}(POP)$;

for $i = 1:n$

for $j = 1: N(i)$

$a = \text{find}(POP(i,:) = j)$;

$x = \text{length}(a)$;

if $(x/m) < p_m$

$[s, y] = \text{sort}(\text{neighbor}(:, a))$;

$POP(i, a) = y(l)$; $y(l) \neq a$, $l = 2, \dots, L$

endif

endfor

endfor

Step3: Return POP.

3.2.6. Antibody update operator

The antibody operator helps prevent overcrowding of antibodies and maintains diversity within the population. Individuals

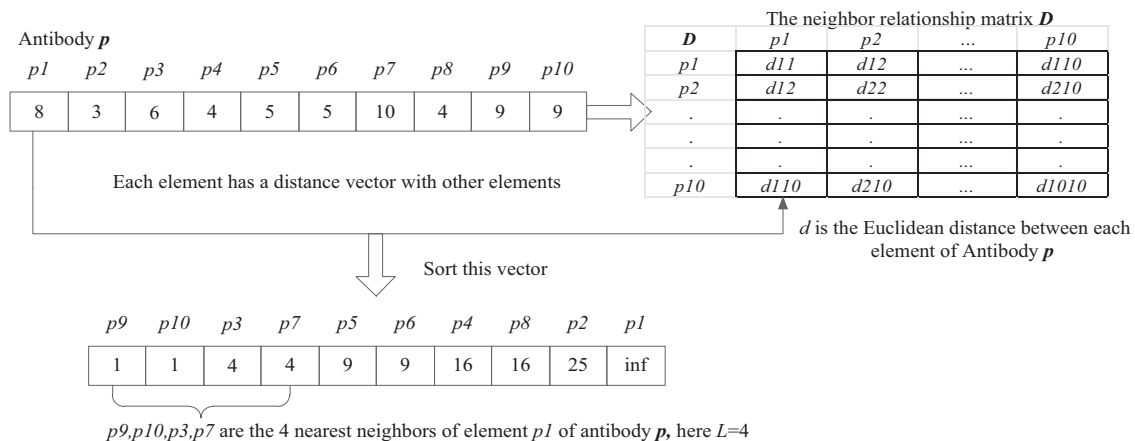


Fig. 2. The rule of neighborhood relations.

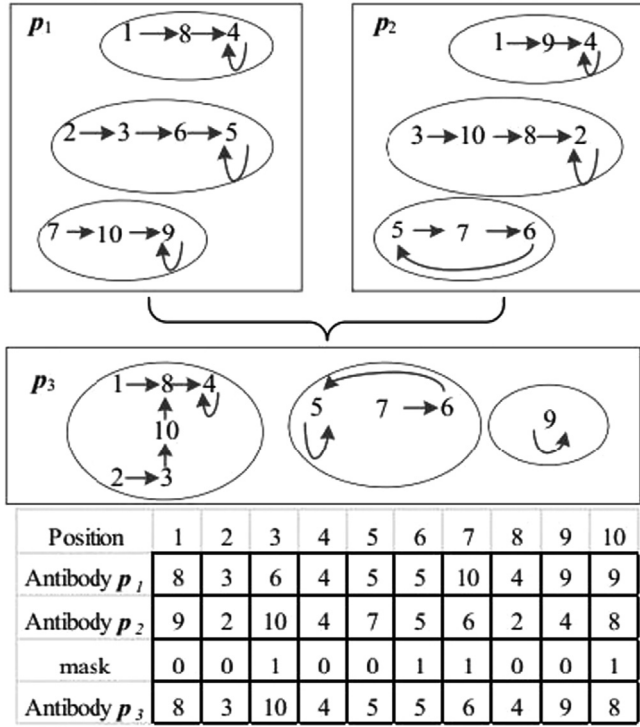


Fig. 3. Uniform crossover operator.

enter into the next generation, depending on whether or not they are non-dominated. During the clone operator stage, there may be many non-dominated solutions in one generation; therefore, the scale of the non-dominated solutions can increase rapidly in successive iterations. During successive generations, increasing numbers of non-dominated antibodies can be selected, reducing the diversity of the population and potentially reducing the speed of convergence. The update operator ensures that when the number of the non-dominated antibodies reaches a certain threshold after clone selection, the most crowded antibodies in the Pareto front will be deleted to ensure that solutions are well spread out along the Pareto front. Thus, this operator helps maintain the diversity of the antibody population (Shang et al., 2012), which improves the speed of convergence. The antibody operator is shown in Algorithm 2.

Algorithm 2. Antibodies update operator

Preparation: The current population set represents

$$P = (p_1, p_2, \dots, p_n).$$

The number of antibodies n .

The number of the expected antibodies m .

The antibody objective functions of antibody x :

$$F(x) = \{(f_{11}(x), f_{12}(x)), (f_{21}(x), f_{22}(x)), \dots, (f_{n1}(x), f_{n2}(x))\}.$$

Step1: Initialization: $F(n \times 2)$, $i = 1$, i is the number of object functions.

Step2: for $i = 1 : 2$

$$y_{fi} = F(\cdot, i);$$

$$y_{fi} = \text{sort}(y_{fi});$$

$$C_{i1} = \infty; C_{in} = \infty;$$

for $j = 2 : n - 1$

$$C_{ij} = C_{ij} + \frac{y_{fi}(j+1) - y_{fi}(j-1)}{f_{i \max} - f_{i \min}};$$

endfor

endfor

Step3: Delete the antibody which has the minimum fitness function value C_{ij} and get the new antibody population P_1 and

objective function matrix F_1 . Set $n := n - 1$, $P = P_1$, $F = F_1$, if $n = m$, stop and output antibodies, otherwise go to step 1.

3.2.7. Summary of stage 1

In summary, the pseudo-code algorithm for stage 1 is shown in Algorithm 3.

Algorithm 3. Self-adaptive artificial immune multi-objective clustering algorithm

Input: The maximum operating generation $g_{\max 1}$; the initial population $P(0)$; the crossover probability p_c ; the mutation probability p_{m1} ; and the scale of non-dominated antibodies S_1 .

Output: The result of classification.

Step1: Raw classification: Classify the difference image by watershed transformation.

Step2: Initialization: Initialize population $P(0)$ by mapping the results of watershed segmentation with the neighbor relationship based antibody link mechanism and initialize the iteration number $t = 0$.

Step3: Calculate the affinity: Calculate the affinity of the antibodies by Eqs. (7) and (8).

Step4: Clone operator: Find non-dominated antibody population, perform cloning on the selected S_1 antibodies and generate population $P_c(t)$.

Step5: Immune operator: Perform uniform crossover and neighbor-based mutation operators for population $P_c(t)$ and generate population $P_r(t)$.

Step6: Antibody update operator: Update population $P_r(t)$

Step7: Stop condition judgment: If $t \leq g_{\max 1}$, $t = t + 1$ and go to step 2, otherwise output the current antibody population.

3.3. Stage 2: classification of uncertain pixels from texture features using immune clonal multi-objective clustering algorithm

During stage 1 (Section 3.2), the difference image is rapidly divided into three classes (changed, unchanged and uncertain samples) with low computational cost, by using the most simple features of pixel gray-levels. In stage 2, any remaining uncertain samples from stage 1 are further analyzed by an immune clonal multi-objective clustering algorithm using (more expensive but more discriminating) texture features derived from wavelet decomposition.

3.3.1. Texture feature extraction

Popular methods for parameterizing and extracting texture features include gray level cooccurrence matrix (GLCM) (Haralick et al. 1973), wavelet decomposition (Hu et al., 2001) and a variety of other methods. Here we adopt wavelet decomposition, because it extracts multi-scale image information and makes full use of local time–frequency characteristics, multi-scale variation characteristics and direction features. The non-subsampled wavelet transform is shown in Fig. 4.

Fig. 4 shows the four subimages which are obtained by wavelet decomposition of the image. In Fig. 4, H and L represent the high-pass and low-pass filters. LL subimage is obtained by the transverse and longitudinal low-pass filter. The subimages of LH, HL and HH contain high frequency component.

We use the l_1 norm and average deviation as the measures of texture. The definitions of these features are

$$e = \frac{1}{M \times N} \sum_{m=1}^M \sum_{n=1}^N |\omega(m, n)| \quad (11)$$

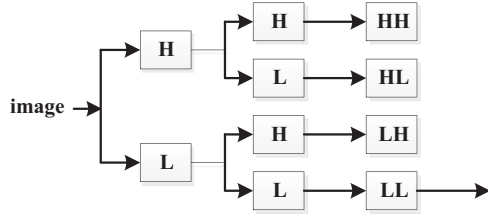


Fig. 4. Non-subsampled wavelet transform.

where $M \times N$ is the size of image, and m and n represent the row and the column of the image, respectively. ω stands for wavelet coefficient. The dimension of feature vector is $D = 3 \times L + 1$. L is the selection of decomposition level of wavelet. In experiments, we adopt three levels of wavelet decomposition and a 15×15 sliding window is used to get feature vectors $(e_{LL-1}, e_{LH-1}, e_{HL-1}, e_{HH-1}, e_{LH-2}, e_{HL-2}, e_{HH-2}, e_{LH-3}, e_{HL-3}, e_{HH-3})$. Once texture feature values have been assigned to each pixel of the difference image, classification of any remaining uncertain pixels proceeds as follows.

3.3.2. Initialization

Fig. 5 illustrates how an antibody can encode a candidate solution for the location of cluster centers for each class. k is the number of categories and m is the dimension of each clustering center, i.e., the dimension of texture features.

At iteration $t = 0$, population $\mathbf{Q}(0)$ is initialized randomly. At each subsequent iteration t , antibody groups $\mathbf{Q}(t) = [\mathbf{q}_1(t), \mathbf{q}_2(t), \dots, \mathbf{q}_y(t)]^T$ are obtained and are regarded as candidate solutions.

3.3.3. Affinity

Two fuzzy clustering indices XB and JM are adopted as the affinity function. Maulik and Bandyopadhyay (2002) proved that XB and JM indicators find a set of non-dominated antibodies which are mutually exclusive and complementary. Yang et al. (2011) showed how these two indices could be successfully used with an artificial immune multi-objective clustering algorithm to segment images. XB and JM can be defined as

$$g_1(\mathbf{q}_m(t)) = \text{JM} = \sum_{j=1}^H \sum_{n=1}^K \mu_{nj}^2 \|\mathbf{x}_j - \mathbf{q}_{mn}(t)\|^2 \quad (12)$$

$$g_2(\mathbf{q}_m(t)) = \text{XB} = \frac{\sigma}{H} \times \frac{1}{d_{\min}} \quad (13)$$

where

$$\sigma = \sum_{n=1}^K \sum_{i,j=1}^H \mu_{ij}^2 \|\mathbf{x}_j - \mathbf{q}_{mn}(t)\|^2, \quad d_{\min} = \min_{i,j=1, \dots, K, i \neq j} \|\mathbf{q}_{mi}(t) - \mathbf{q}_{mj}(t)\|^2,$$

and $\mathbf{q}_m(t)$ is the m -th antibody of the antibody population at the t -th iteration. K is the number of classes. H is the number of pixels in the image. \mathbf{x}_j ($j = 1, 2, \dots, H$) is the characteristic vector of pixels. $\mathbf{q}_{mn}(t)$ ($n = 1, 2, \dots, K$) is the clustering center of each class at the t -th iteration. μ_{nj} is the fuzzy membership.

In Eq. (13), XB is a densification–separation effectiveness function and it describes the ratio between the sum of fuzzy mean square distance and the minimum distance between clustering centers. Small values of XB indicate better partition. In Eq. (12), the JM indicator is the sum of overall pixels fuzzy mean square distance. It can be seen that JM is a measure of pixel classification index, and XB is the product of the JM and the minimum distance of the nearest neighbor between classes. Thus, XB's minimization depends on the minimization d_{\min} of JM and the maximization of the separability of the nearest neighbor classes. Therefore, it is generally difficult to find minimum solutions of XB and JM simultaneously, and so a set of non-dominated solutions is obtained.

3.3.4. Selection and cloning

For stage 2, the selection operator and clone operator are the same as those used in stage 1, see Sections 3.2.3 and 3.2.4.

3.3.5. Immune operators

In immunology, mutation is the main operator of the affinity maturation. In this stage, non-uniform mutation is used to change the components of antibodies. Non-uniform mutation uses local search to improve the affinity between antibodies and antigens, generating improved solutions. Moreover, it makes the range of variation relatively large in the early evolution iterations. With the development of evolution (successive iterations), the range of variation will become smaller and smaller, providing a fine tuning role in the evolution procedure.

3.3.6. Antibody update

The antibody update operator is the same as that used in stage 1, described in Section 3.2.6.

3.3.7. Summary of stage 2

In summary, the process of second part algorithm is shown in Algorithm 4.

Algorithm 4. Immune clonal multi-objective clustering algorithm

Input: The sample category number k ; the maximum operating generation $g_{\max 2}$; the initial population $\mathbf{Q}(0)$; the non-dominated antibody scale S_2 ; and the mutation probability p_{m2} .

Output: Clustering centers.

Step 1: Initialization: Initialize the population $\mathbf{Q}(0)$, the iteration number $t = 0$ and the category number k .

Step 2: Calculate affinity: Calculate the affinity g_1 and g_2 by Eqs. (13) and (14).

Step 3: Clone operator: Find non-dominated antibodies, perform cloning on the selected S_2 antibodies at different ranks and generate new population $\mathbf{Q}_c(t)$.

Step 4: Immune operator: Perform non-uniform mutation with probability p_m and generate a new population $\mathbf{Q}_r(t)$.

Step 5: Antibody update operator: Update population $\mathbf{Q}_r = (t)$.

Step 6: Iteration terminal condition: If $t \leq g_{\max 2}$, $t = t + 1$, and go to step 2, otherwise output the current antibody population.

3.4. Summary of the two-stage change detection method

The specific steps of the change detection method are shown in Algorithm 5.

Algorithm 5. Artificial immune multi-objective clustering based SAR image change detection.

Input: Two SAR images I_{t1} and I_{t2} .

Output: Result image.

Step1: Use SAR images I_{t1} and I_{t2} to generate a difference image DI (see Section 4.2 for details).

Step2: Perform initial segmentation of DI pixels into three classes (changed, unchanged, and uncertain) using only pixel gray level features, by using self-adaptive artificial immune multi-objective clustering method. Its implementation procedure is shown in Section 3.2.

Step3: Extract textural features of image DI by using wavelet decomposition.

Step4: Calculate clustering centers of the uncertain samples in the high dimensional wavelet texture feature space c , by

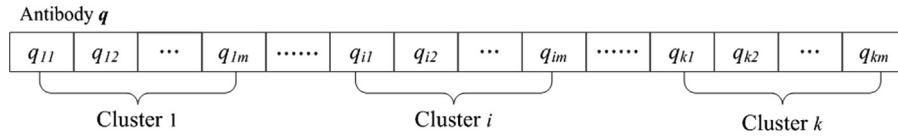


Fig. 5. An antibody encodes a candidate solution for the set of k class cluster centers of m dimensions.

using the immune clonal multi-objective clustering method. Its implementation procedure is shown in Section 3.3.

Step5: Classify the uncertain samples by Euclidean distance and use the third evaluation index to select the optimal solution. The third index is expressed as

$$f = \sum_{r=0}^1 \frac{T_r}{M \times N} \sum_{\forall(i,j) \in R_r} (DI(i,j) - \mu_r)^2 \quad (14)$$

where $M \times N$ is the size of the image. T_r represents the number of unchanged or changed pixels. R_r is a set of pixels. $DI(i,j)$ is the grayscale pixel values of the difference image. μ_r is the mean gray value of changed or unchanged classes.

4. Experimental results

4.1. Description of experimental data sets

In order to show the effectiveness of the proposed method for SAR image change detection, we have tested it on four publicly available ground truth data sets which are popular in the literature and have been used to test a variety of other important methods for SAR image change detection. This allows our method to be seen in the context of other key papers from the literature.

The first data set is a section (350×290 pixels) of two SAR images over the city of Ottawa acquired by the Radarsat SAR sensor. The changed areas of the two SAR images are mainly due to the onset of the rainy season, in May and August 1997, the ground-truth for the changed number of target pixels is the 16049.

The second data set was acquired over an area near the city of Bern by the European Remote Sensing 2 satellite SAR sensor in April and May 1999. The size of these two images is 301×301 . Ground changes are due to the River Aare flooding large parts of the cities. The changed number of target pixels is 1155.

The third and fourth data sets were acquired by Radarsat-2 at the region of Yellow River Estuary in China in June 2008 and 2009. The image of 2008 was acquired as a single visual image. The image of 2009 was composed from four visual images. Thus, the images at the earlier and later dates have very different noise levels. This phenomenon leads to a complex process of change detection, but also can reveal useful observations about the performance of the proposed method. Because these two 7666×7692 SAR images are too large to show the detailed information of change areas, we have selected two areas of size 257×289 and 306×291 to test the proposed method.

4.2. Choice of image differencing method

For the performance of SAR image change detection, the quality of the difference image is very important. The subtraction operator and the ratio operator are well-known methods for producing a difference image. However, the ratio operator is more suitable for SAR images, where the ratio difference image usually comprises log-ratio and mean-ratio images (Rignot and Van Zyl, 1993). In many literatures, both methods have yielded effective results for SAR image change detection. In this paper, mean-ratio (Gong et al., 2012) is used to generate the difference image.

$$DI = 1 - \min \left(\frac{\mu_1}{\mu_2}, \frac{\mu_2}{\mu_1} \right) \quad (15)$$

where μ_1 and μ_2 represent the local mean values of multi-temporal SAR images.

4.3. Comparison against other methods

Our experiments evaluate the proposed method and compare it against four other well known methods from the literature. These are:

- (1) Change detection in satellite images using a genetic algorithm (GA) approach (Celik, 2010b). This contrast method uses an evolutionary algorithm with a single objective to deal with image change detection. Comparatively performance of this approach confirms the necessity of the two step algorithm in our proposed method.
- (2) Change detection for SAR images based on quantum-inspired immune clonal clustering (QICC) algorithm (Li et al., 2011). This contrast method uses an immune clonal clustering algorithm with a single objective to deal with image change detection. Therefore, its deficiencies support our claims for the effectiveness of our multi-objective clustering method.
- (3) Image change detection using the Gaussian mixture model and the genetic algorithm (GMGA) (Celik, 2010a). Comparison with this method is used to support our choice of artificial immune methods over GA methods.
- (4) Our fourth comparison method is the same as the proposed method, except that the second part is modified to use a K -means algorithm based on the difference image gray levels to search the optimal clustering centers for uncertain samples. This contrast method self-adaptive immune multi-objective pre-processing+ K -means (SIMP+ K -means) is used to verify the effectiveness of the second step algorithm of the proposed method and to confirm the necessity of using texture features in this second step.

4.4. Experimental parameter settings

The parameters in the proposed method and four contrast methods are used as follows:

- (1) Genetic algorithm (GA) method (Celik, 2010b): population consists of 20 individuals, crossover rate is 0.8, mutation rate is 0.01, and the largest number of iterations is 200,000.
- (2) Quantum-inspired immune clonal clustering (QICC) method (Li et al., 2011): population consists of 20 individuals.
- (3) Image change detection using the Gaussian mixture model and genetic algorithm (GMGA) (Celik, 2010a): $\beta = 1.67$.
- (4) SIMP+ K -means method: population consists of 20 individuals, the scale of clone is 40, and the maximal number of iterations is 100, crossover rate is 0.8, mutation rate is 0.01.
- (5) The proposed method: population consists of 20 individuals, crossover rate is 0.8, the first mutation rate is 0.01, the second mutation rate is 0.1, the scale of clone is 40, and the maximal number of iterations is 100.

The values of parameters of GMGA, GA and QICC methods adopt the best values in the literatures (Celik, 2010a, 2010b; Li et al., 2011). In order to compare with GMGA, GA and QICC methods, some values of parameters of SIMP+ K -means and the

proposed method are set to be the same as for the comparison methods, and others are justified empirically in the experiments.

4.5. Evaluating indicators

In order to evaluate the result of detection, four indicators are used to evaluate the quality of the results (Rosenfield and Fitzpatrick-Lins, 1986). Im is the reference image. I is the result image.

- (1) False Positive (FP) number: unchanged pixels wrongly judged as changed pixels. It is defined by

$$FP = \sum_{i=1}^{N_{total}} u_i \quad (16)$$

where

$$u_i = \begin{cases} 1 & \text{if unchanged pixel } x_i \text{ is judged as changed one} \\ 0 & \text{others} \end{cases}$$

N_{total} is the total number of the unchanged image pixels.

- (2) False Negative (FN) number: changed pixels that missed detection. It is defined by

$$FN = \sum_{i=1}^{M_{total}} v_i \quad (17)$$

where

$$v_i = \begin{cases} 1 & \text{if unchanged pixel } x_i \text{ is judged as changed one} \\ 0 & \text{others} \end{cases}$$

M_{total} is the total number of the changed image pixels.

- (3) Overall error (OE) number: the sum of the number of unchanged pixels wrongly judged as changed pixels and the number of changed pixels wrongly judged as unchanged pixels, i.e., the sum of FP and FN. It is defined by

$$OE = FP + FN \quad (18)$$

- (4) kappa coefficient: it is a measure of classification accuracy index based on difference between error matrix and chance agreement. The closer to 1 the value is, the more approximate to the real classification the results are. It is defined by

$$\text{kappa} = \frac{P_a - P_e}{1 - P_e} \quad (19)$$

where

$$P_a = \frac{TN - TE}{TN}, \quad P_e = \frac{(T_a + FN)(T_a + FP)}{TN^2} + \frac{(T_b + FN)(T_b + FP)}{TN^2},$$

$$T_a = TN - FN, \quad T_b = TN - FP$$

and TN is the total number of pixels.

Note: for the problem of change detection, small values of FP, FN and OE indicate good results (accurate change detection). In contrast, high values of kappa indicate good results.

4.6. Results and analysis

The experiment results on four data sets are shown and analyzed as follows:

4.6.1. Results and analysis on the Ottawa data set

In the first data set experiment, in order to validate the effectiveness of the proposed method on the results of SAR-image change detection, a comparison analysis is carried out on four difference methods which are GMGA, GA, QICC and

SIMP+K-means. The change detection results of the Ottawa data by five different methods are shown in Fig. 6.

Fig. 6(e) is the classification result by SIMP (the first stage of our proposed two-stage method). The difference image is divided into three classes. The gray pixels stand for uncertain samples. The white pixels represent changed class and the black pixels belong to the unchanged class. It can be seen from Fig. 6(f) and (g) that the change detection results achieved by GA and QICC, which adopt a single objective function with the evolutionary algorithm, contain lots of false change information. This can be explained by the tendency of these two methods to converge on local optima and their inability to consider information about spatial context and texture information. In contrast, by considering the multi-objective optimization and the features of local information, the change detection results generated by SIMP+K-means [Fig. 6(i)] and the proposed method [Fig. 6(j)] reduces the false change information and are much closer to the ground truth reference image. In Fig. 6(i), by using gray value information of difference image to classify uncertain samples, the change detection result reduces the false change regions, but still fails to detect fine details of change information. In contrast, by using texture information and a multi-objective evolutionary algorithm to classify uncertain samples, the best result is obtained as illustrated in Fig. 6(j). It reduces the false change errors and produces results much closer to the ground truth reference image. Fig. 6(h) is obtained by the method for SAR image change detection using GMGA where a genetic algorithm is used to estimate the parameters of a Gaussian mixture model. This method uses a statistical model to realize change detection. As shown in Fig. 6(h), the GMGA method can generate better results than GA and QICC, but due to the speckle noise of SAR images, GMGA gets worse result than the proposed method.

In order to illustrate the effectiveness of the proposed method, the quantitative results of SAR image change detection are shown in Table 1. It describes the results of FP, FN, OE and kappa by these different methods on the Ottawa data set.

It can be seen from Table 1, compared with other four methods, the change detection result of GA is the worst and FP and FN are higher than the proposed method. Compared with GA, QICC, GMGA and SIMP+K-means methods, FP of the proposed method is lower than the four comparison methods; however FN is significantly higher than the other methods except for GA. The low FP rate for our method can be explained by the fact that GMGA, QICC and SIMP+K-means only use grayscale pixel values of the difference image, but the proposed method additionally makes use of texture features of the difference image, which reduces the noise and the detail information. Therefore, the number of FP of the proposed method is reduced compared to other methods. But the FN is increased. For the coefficient of OE which is the sum of FP and FN, the smaller value of OE, the better the result. And for the coefficient of kappa, the closer to 1 the kappa is, the better the method is. It can be seen from Table 1, GA has the lowest value of kappa, but GMGA, QICC, SIMP+K-means and the proposed method have the higher kappa (0.8957 for QICC, 0.9195 for GMGA, 0.9375 for SIMP+K-means and 0.9427 for the proposed method). The proposed method generates the highest kappa (0.9427) and the lowest OE (1565), suggesting that it outperforms the other methods overall. The reason why our proposed method shows increased FN errors may be that the additional features suppress useful edge information at the same time as suppressing harmful speckle noise.

4.6.2. Results and analysis on the Bern data set

Fig. 7 represents the results of five methods for the Bern data. Fig. 7(d) is the difference image. Fig. 7(e) is the classification result

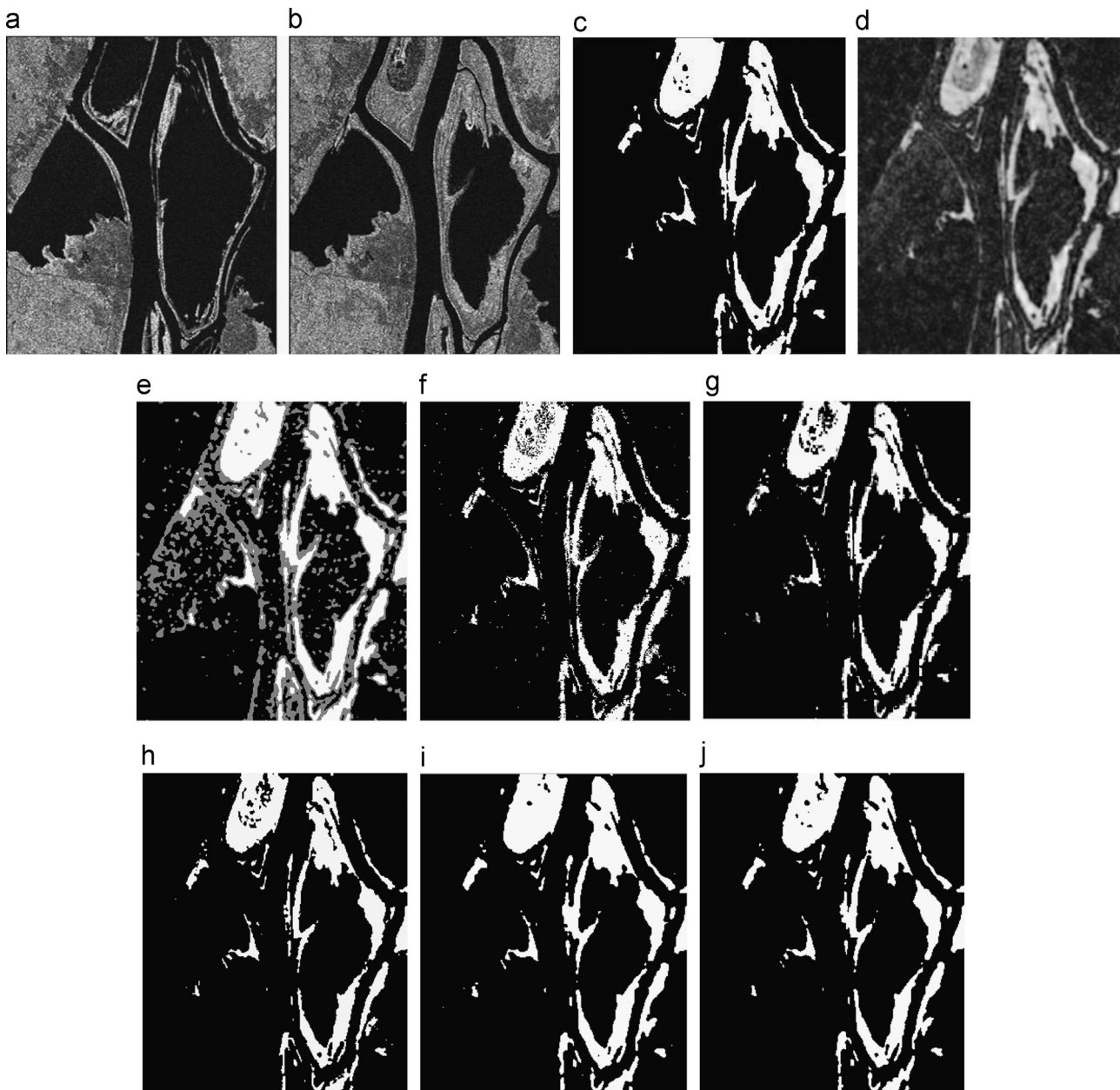


Fig. 6. Experiment results of the Ottawa data set. Images acquired (a) before and (b) after the flood. (c) Ground truth. (d) The difference image. (e) The result of classification by SIMP. (f) GA. (g) QJCC. (h) GMGA. (i) SIMP+K-means. (j) The proposed method.

Table 1
Simulation results of FP, FN, OE and kappa by five methods on the Ottawa data set.

Data set	Method	FP	FN	OE	Kappa
Ottawa	GA	2232	1004	3236	0.8764
	QJCC	1971	299	2270	0.8957
	GMGA	1976	96	2072	0.9195
	SIMP+K-means	1221	434	1655	0.9375
	The proposed method	577	988	1565	0.9427

Best results in bold.

by SIMP (the first stage of our proposed two-stage method) which divides the difference image into three classes, where the gray pixels represent uncertain samples. The second stage of both SIMP+K-means and our proposed method make use of these uncertain pixel labels. In Fig. 7(f), the result of change detection has lots of spots of false detections. This phenomenon can be

explained because GA fails to take account of the image speckle noise and also uses only a single feature. It does not take into account context information and multi-objective optimization. Figs. 7(g), 6(h) and 5(i), show that QJCC reduces the amount of missing information (FN false negatives) while GMGA and SIMP+K-means reduce patches of FP false detections. The proposed algorithm appears to be the most resistant to noise, thereby reducing the error rate and preserving the detailed information of the change detection.

The simulation results of FP, FN, OE and kappa by the five methods on the Bern data set are shown in Table 2. The change detection result of GA is the worst. GMGA, QJCC and SIMP-K-means result in higher kappa (0.8438 for GMGA, 0.8018 for QJCC and 0.8482 for SIMP-K-means) than GA. The maximum kappa (0.8514) and the lowest FP (313) are acquired by the proposed method, which shows the suitability and stability of the proposed method overall.

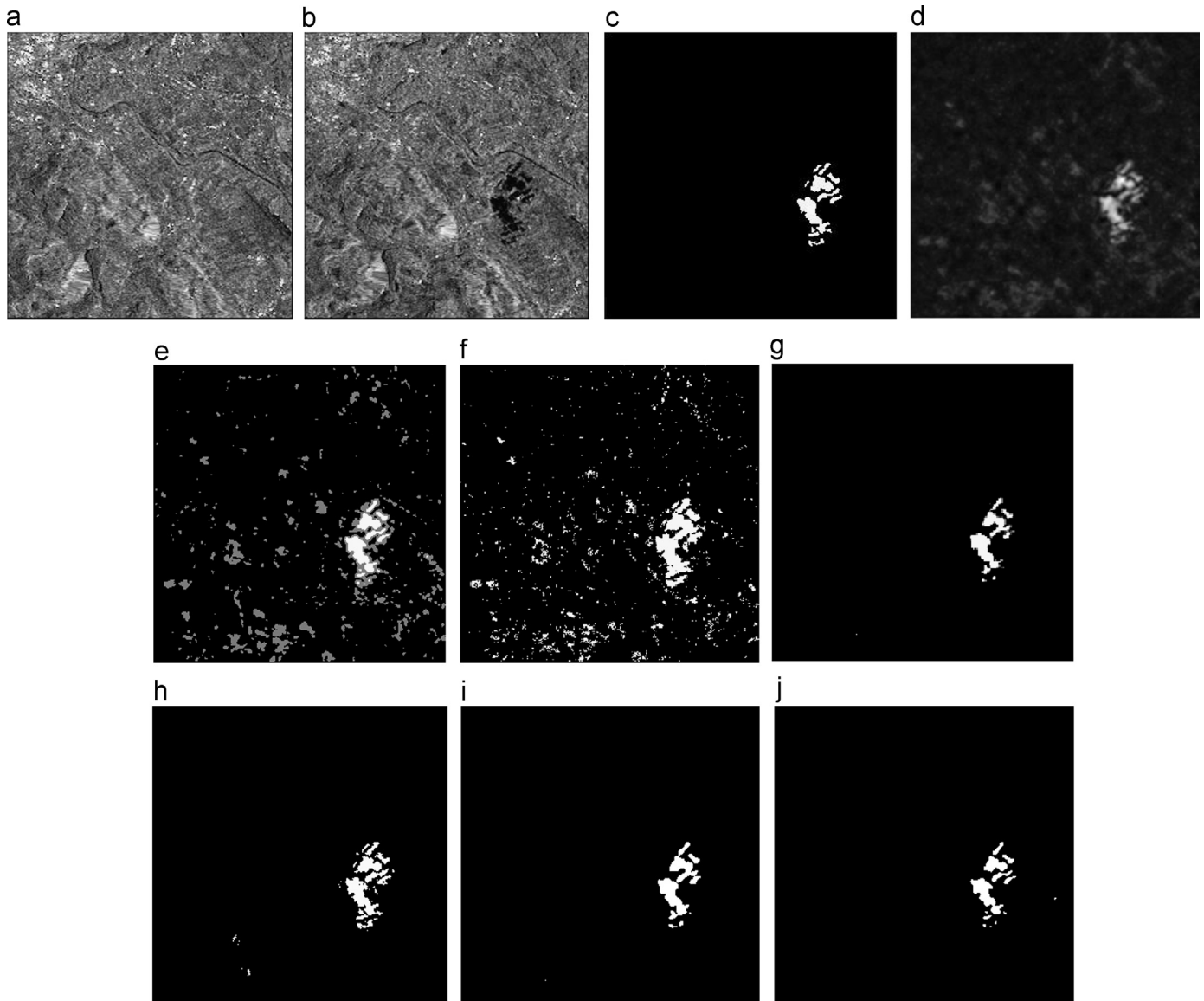


Fig. 7. Experiment results of the Bern data set. Images acquired (a) before and (b) after the flood. (c) Ground truth. (d) The difference image. (e) The result of classification by SIMP. (f) GA. (g) QICC. (h) GMGA. (i) SIMP+K-means. (j) The proposed method.

Table 2
Simulation results of FP, FN, OE and kappa by five methods on the Bern data set.

Data set	Method	FP	FN	OE	Kappa
Bern	GA	3019	19	3038	0.4165
	QICC	294	98	392	0.8018
	GMGA	269	90	359	0.8438
	SIMP+K-means	188	162	350	0.8482
	The proposed method	67	246	313	0.8514

Best results in bold.

4.6.3. Results and analysis on the HuangHe1 data set

In the third data set, we use more complicated data in which the speckle noise in Fig. 8(b) (the image from the earliest date) is much greater than Fig. 8(a) (the image from the later date) to analyze the suitability of the proposed approach. The change detection results obtained by five methods for the HuangHe1 data set are shown in Fig. 8.

It can be seen from Fig. 8 that the change detection result obtained by GA has lots of FP false positive errors as illustrated in Fig. 8(f). On the other hand, in Fig. 8(i), much information is lost as

FN false negative errors by SIMP+K-means, although this method does improve over GA in terms of less FP false positive errors. In Fig. 8(g), the QICC method has generated a large amount of FP false positive errors. As shown in Fig. 8(h), the proposed method has less noise, significantly reduces the FP false positive errors, and is much closer to the ground truth.

Table 3 gives the results of FP, FN, OE and kappa by five methods on the HuangHe1 data set.

As shown in Table 3, the proposed method results in the highest kappa and the lowest FP and OE. These quantitative results on the HuangHe1 data set show that the proposed method significantly outperforms the comparison methods overall.

4.6.4. Results and analysis on the HuangHe2 data set

The fourth data set has similar complex data as in the third data set, with significantly differing noise levels in the images from the two time steps. The change detection results by the five different methods for the HuangHe2 data set are shown in Fig. 9. The change detection result obtained by GA has lots of FP false positive errors as illustrated in Fig. 9(f). Fig. 9(g)–(i) also shows significant

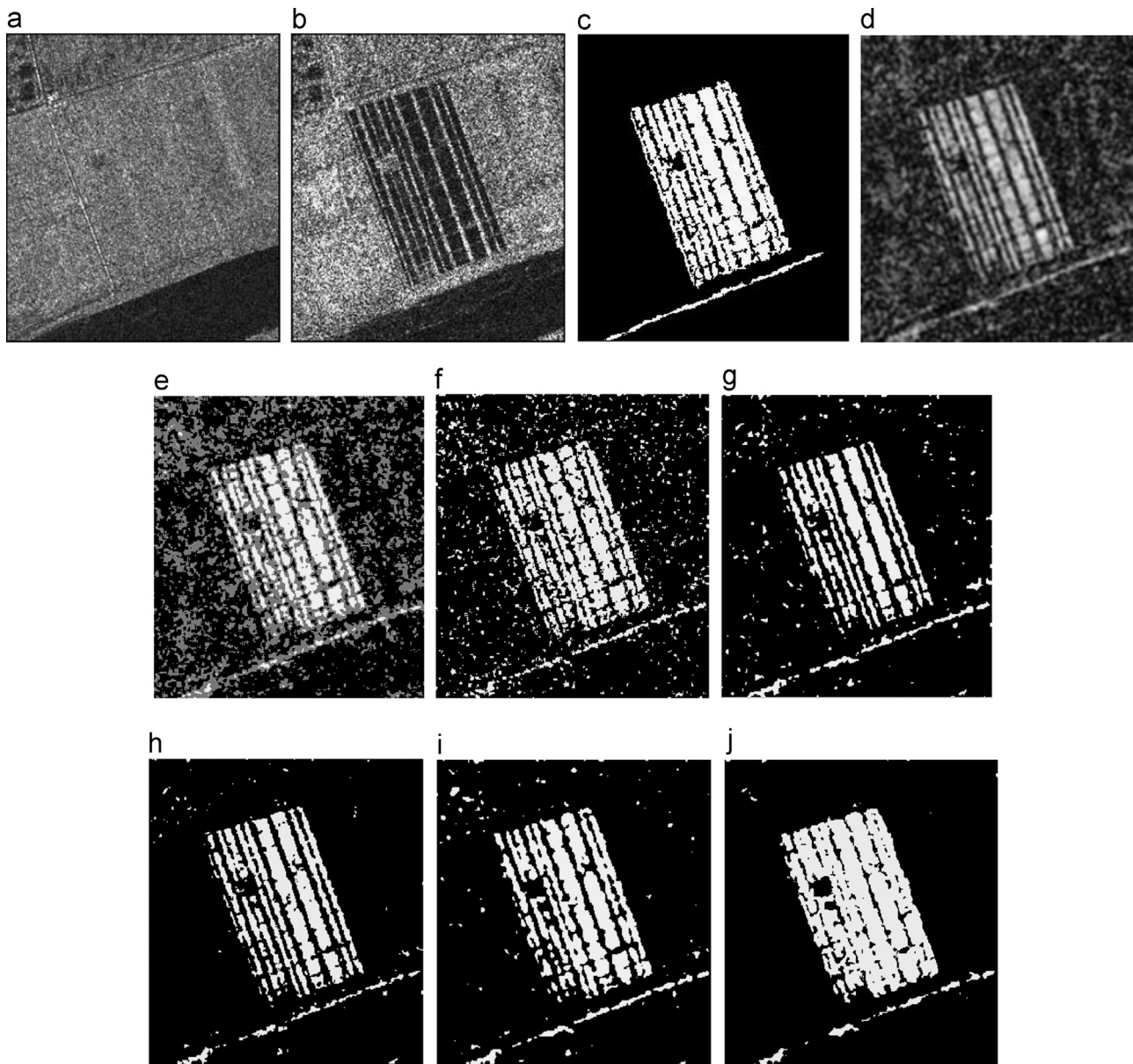


Fig. 8. Experiment results of the HuangHe1 data set. (a) Image acquired in June 2008. (b) Image acquired in June 2009. (c) Ground truth. (d) The difference image. (e) The result of classification by SIMP. (f) GA. (g) QICC. (h) GMGA. (i) SIMP+K-means. (j) The proposed method.

Table 3
Simulation results of FP, FN, OE and kappa by five methods on the HuangHe1 data set.

Data set	Method	FP	FN	OE	Kappa
HuangHe1	GA	4020	2610	6630	0.7039
	QICC	4146	1734	5880	0.7047
	GMGA	3943	683	4642	0.7610
	SIMP+K-means	3087	1250	4337	0.7862
	The proposed method	1279	2514	3793	0.8297

Best results in bold.

false positive errors. It can be seen from Fig. 9(j), that the proposed method has less noise, reduces false positive errors, and is much closer to the ground truth.

The results of FP, FN, OE and kappa by these different methods on HuangHe2 data set are shown in Table 4. As shown in Table 4, the proposed method results in the highest kappa and the lowest

FP and OE which show the effectiveness and the suitability of the proposed method.

It can be seen from the simulation results that the proposed method can obtain a higher accuracy rate at difference levels of noise of multi-temporal SAR images. Therefore, it can be concluded that the proposed method shows improved robustness to noise.

From the results of experiments above it can be seen that the proposed method can effectively achieve better detection results with a high rate of precision. Due to the speckle noise of SAR image, the grayscale pixel values of the difference image are influenced by noise, thus many pixels are misclassified by techniques which rely only on grayscale values. In contrast, texture features can overcome the influence of speckle noise. Therefore, the number of FP of the proposed method is reduced compared to other methods, but the number of FN has increased a lot. Therefore, our method may be less well suited to particular applications where FN errors are considered more important than FP errors. The reason why our proposed method shows increased FN errors

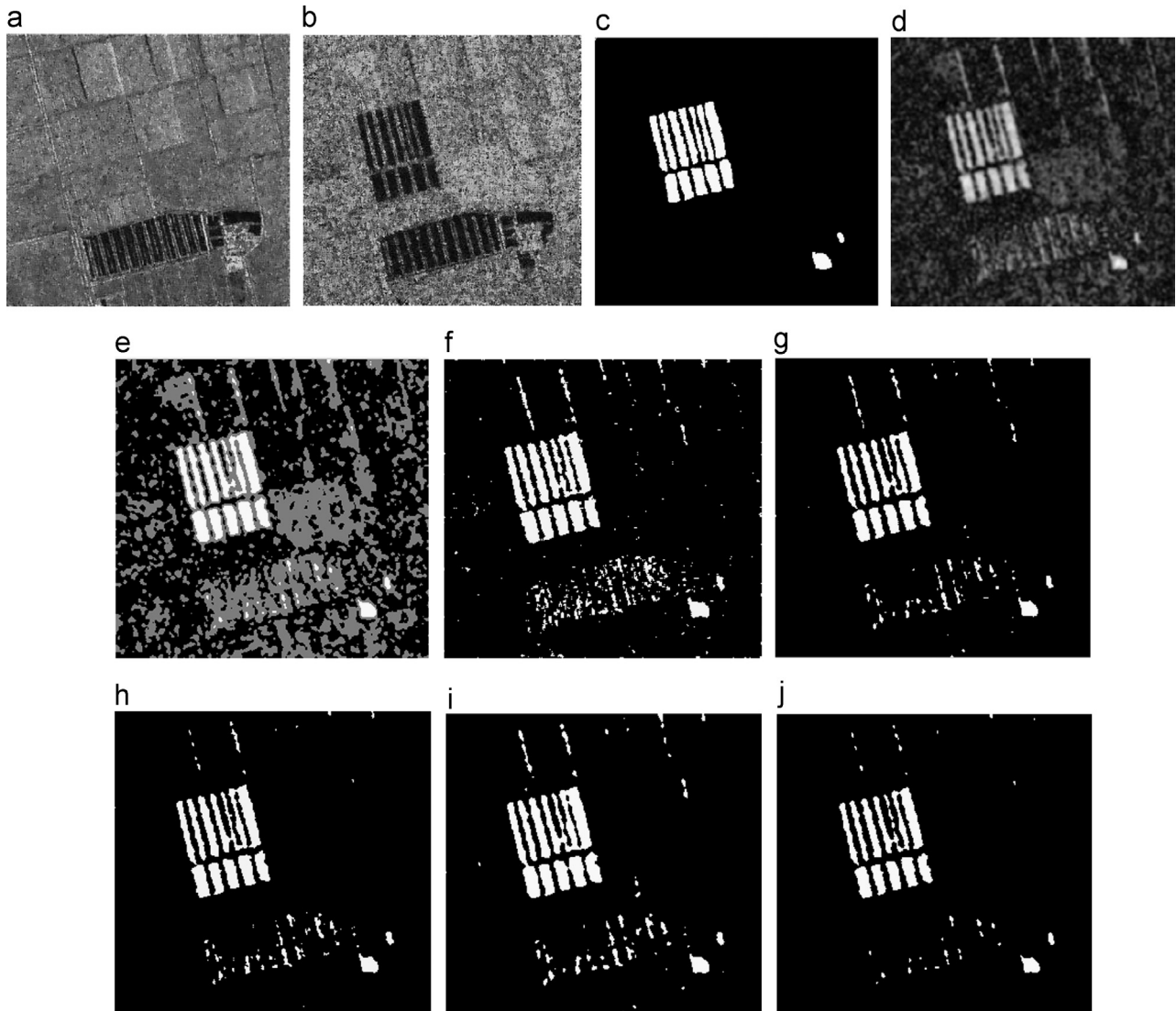


Fig. 9. Experiment results of the HuangHe2 data set. (a) Image acquired in June 2008. (b) Image acquired in June 2009. (c) Ground truth. (d) The difference image. (e) The result of classification by SIMP. (f) GA. (g) QICC. (h) GMGA. (i) SIMP+K-means. (j) The proposed method.

Table 4

Simulation results of FP, FN, OE and kappa by five methods on the HuangHe2 data set.

Data set	Method	FP	FN	OE	Kappa
HuangHe2	GA	2096	644	2740	0.7553
	QICC	1213	837	2050	0.7861
	GMGA	1046	776	1822	0.8081
	SIMP+K-means	1217	768	1985	0.8175
	The proposed method	284	1422	1706	0.8415

Best results in bold.

may be that the additional features suppress useful edge information at the same time as suppressing harmful speckle noise.

4.7. The running time comparison analysis

Table 5 shows the mean running time of GA, QICC, GMGA, SIMP+K-means and the proposed method on the test images. These five methods are implemented in Matlab R2013a on HP dc7800 (Intel(R) Core(TM) 2 Duo CPU and the system of Microsoft Windows 7).

Table 5

The mean running time of GA, QICC, GMGA, SIMP+K-means and the proposed method.

Methods	GA	QICC	GMGA	SIMP+K-means	The proposed method
Times(s)	31,020.472	46.816	97.546	298.303	1856.376

It can be seen from Table 5 that GA requires the longest running time and gets the worst result. The reason may be that the size of the images is too large and GA regards the results as initial population directly and uses the genetic algorithm to search the minimum solution of fitness function as change detection result in all possible directions. Therefore, the convergence speed of GA is slow. QICC is the lowest in computational times. GMGA and SIMP+K-means also have less running time. However, they cannot get the best detection accuracy. The running time of the proposed method is only less than GA and more than other three methods. It can be explained that the main computational load of the five methods lie in the antibody initialization, antibody selection and population iterations. What is encouraging is that the proposed method adopts the best detection results compared with QICC,

GMGA, and SIMP+K-means. Additionally, the running time of the proposed method could be reduced greatly by initialization compared with GA. Therefore, the proposed method can obtain a balance between the computational time and the detection accuracy.

5. Conclusion

In this paper, a novel unsupervised change detection method for SAR images based on artificial immune multi-objective clustering has been proposed. This method treats the change detection problem as multi-objective optimization problem. The key idea is to use gray value and texture characteristics of the difference image with an artificial immune multi-objective optimization algorithm respectively to classify the difference image. Its procedure is divided into two stages. Both of these two stages use the artificial immune multi-objective clustering algorithm, but they have different goals, different encoding mechanisms and different operators and use different informations.

These two stages can be described as follows: First, the self-adaptive artificial immune multi-objective algorithm is used to pre-sort the difference image, using gray scale data alone. It outputs those pixels for which an initial segmentation category is uncertain. The second stage exploits the non-subsampled wavelet transform features of the difference image, and uses an immune clonal multi-objective clustering algorithm is adopted to classify uncertain samples, which can efficiently search optimal clustering centers of uncertain samples and improve the local search ability.

The experimental results on four groups of SAR images have evaluated the effectiveness of the proposed method, and the results show that the proposed method can effectively improve the accuracy of image change detection results. Moreover, the evaluation of detection performance illustrates that the proposed method can detect fine detail information more accurately, reduce the false detection rate and achieve detection results with a high detection rate.

In summary, the method of this paper has effectively combined the multi-objective optimization algorithm with artificial immune system, successfully applied to SAR image change detection and realized the self-optimization, self-learning of the method with simple information.

The encoding mechanism, choice of objective functions and feature extraction all play key roles in the proposed method. Once suitable objective functions and features are proposed, the complication of method can be reduced, and this method may be can realized by one step. Currently, many methods of extracting features from difference images have been proposed, there is still no single unified method which can successfully be applied to all SAR image data, obtained by different devices, for detecting change while overcoming speckle noise. Although methods which rely solely on grayscale pixel values may be effective for some images, they will fail to work for other images. Therefore, the proposed method is useful in that it shows how to combine the advantages of multiple features within a single image processing tool.

Acknowledgment

We would like to express our sincere appreciation to the anonymous reviewers for their insightful and valuable comments, which have greatly helped us in improving the quality of the paper. This work was partially supported by the National Basic Research Program (973 Program) of China under Grant 2013CB329402, the National Natural Science Foundation of China,

under Grants 61371201, 61001202, 61203303 and 61272279, the National Research Foundation for the Doctoral Program of Higher Education of China, under Grant 20100203120008, the Fundamental Research Funds for the Central Universities, under Grant K5051302028, the Fund for Foreign Scholars in University Research and Teaching Programs (the 111 Project) under Grant B07048, and the Program for Cheung Kong Scholars and Innovative Research Team in University under Grant IRT1170.

References

- Amayr, O., Bouguila, N., 2013. On online high-dimensional spherical data clustering and feature selection. *Eng. Appl. Artif. Intell.* 26 (4), 1386–1398.
- Aydin, I., Karakose, M., Akin, E., 2010. Artificial immune classifier with swarm learning. *Eng. Appl. Artif. Intell.* 23 (8), 1291–1302.
- Bandyopadhyay, S., Maulik, U., Mukhopadhyay, A., 2007. Multi-objective genetic clustering for pixel classification in remote sensing imagery. *IEEE Trans. Geosci. Remote Sens.* 45 (5), 1506–1511.
- Bazi, Y., Melgani, F., Bruzzone, L., Vernazza, G., 2009. A genetic expectation-maximization method for unsupervised change detection in multitemporal SAR imagery. *Int. J. Remote Sens.* 30 (24), 6591–6610.
- Belghith, A., Collet, C., Paul, J., 2013. Change detection based on a support vector data description that treats dependency. *Pattern Recognit. Lett.* 34, 275–282.
- Besag, J., 1986. On the statistical analysis of dirty pictures. *J. R. Stat. Soc. Ser. B (Methodolog.)* 48 (3), 259–302.
- Beucher, S., 1992. The watershed transformation applied to image segmentation. *Scanning Microsc.* 6 (Suppl.), 299–314.
- Celik, T., 2009. Unsupervised change detection in satellite images using principal component analysis and K-means clustering. *IEEE Trans. Geosci. Remote Sens. Lett.* 6 (4), 772–776.
- Celik, T., 2010a. Image change detection using Gaussian mixture model and genetic algorithm. *J. Vis. Commun. Image Represent.* 21, 965–974.
- Celik, T., 2010b. Changed detection in satellite images using a genetic algorithm approach. *IEEE Geosci. Remote Sens.* 7 (2), 386–390.
- Chang, C.C., Tseng, H.E., Meng, L.P., 2009. Artificial immune systems for assembly sequence planning exploration. *Eng. Appl. Artif. Intell.* 22 (8), 1218–1232.
- Coello, C.A., Cortes, N.C., 2002. An approach to solve multi-objective optimization problems based on an artificial immune system. In: *Proceedings of the First International Conference on Artificial Immune Systems*, pp. 212–221.
- Curlander, J.C., McDonough, R.N., 1991. *Synthetic Aperture Radar: Systems and Signal Processing*. Wiley-Interscience, New York.
- Cutello, V., Narzisi, G., Nicosia, G., 2005. A class of Pareto archived evolution strategy algorithms using immune inspired operators for ab-initio protein structure prediction. In: *Proceedings of the Applications on Evolutionary Computing, Evoworkshops 2005, Lecture Notes in Computer Science*. vol. 3449, Lausanne, Switzerland, pp. 54–63.
- Deb, K., 2001. *Multi-Objective Optimization using Evolutionary Algorithms*. John Wiley & Sons, Chichester, UK (ISBN 0-471-87339-X).
- Dempster, A.P., Laird, N.M., Rubin, D.B., 1977. Maximum likelihood from incomplete data via the EM algorithm. *J. R. Stat. Soc. Ser. B (Methodolog.)* 39 (1), 1–38.
- Droste, S., Jansen, T., Wegener, I., 2002. On the analysis of the (1+1) evolutionary algorithm. *Theor. Comput. Sci.* 276 (1), 51–81.
- Dunn, J.C., 1973. A Fuzzy relative of the ISODATA process and its use in detecting compact well-separated clusters. *J. Cybern.* 3, 32–57.
- Geman, S., Geman, D., 1984. Stochastic relaxation, Gibbs distributions, and the Bayesian restoration of images. *IEEE Trans. Pattern Anal. Mach. Intell.*, PAMI 6 (6), 721–741.
- Ghosh, A., Badri, N.S., Lorenzo, B., 2013. Integration of Gibbs Markov random field and hopfield-type neural networks for unsupervised change detection in remotely sensed multitemporal images. *IEEE Trans. Image Process.* 22 (8), 3087–3096.
- Ghosh, A., Mishra, N.S., Ghosh, S., 2011. Fuzzy clustering algorithms for unsupervised change detection in remote sensing images. *Inf. Sci.* 181, 699–715.
- Goldberg, D.E., Holland, J.H., 1988. Genetic algorithms and machine learning. *Mach. Learn.* 3 (2), 95–99.
- Gong, M.G., Zhou, Z.Q., Ma, J.J., 2012. Change detection in synthetic aperture radar images based on images fusion and fuzzy clustering. *IEEE Trans. Image Process.* 21 (4), 2141–2151.
- Hu, Z.L., Guo, D.Z., Sheng, Y.H., 2001. Extracting textural information of satellite SAR image based on wavelet decomposition. *Int. J. Remote Sens.* 5 (6), 423–427.
- Handl, J., Knowles, J., 2007. An evolutionary approach to multiobjective clustering. *IEEE Trans. Evol. Comput.* 11 (1), 56–76.
- Haralick, R.M., Shanmugam, K., Dinstein, I., 1973. Texture features for image classification. *IEEE Trans. Syst. Man Cybern.* 3 (6), 610–621.
- Huang, W.L., Jiao, L.C., 2008. Artificial immune kernel clustering network for unsupervised image segmentation. *Prog. Nat. Sci.* 18 (4), 455–461.
- Kalinli, A., Karaboga, N., 2005. Artificial immune algorithm for IIR filter design. *Eng. Appl. Artif. Intell.* 18 (8), 919–929.
- Li, Y., Wu, N., Jiao, L.C., 2011. Change detection for SAR images based on quantum-inspired immune clonal clustering algorithm. *J. Infrared Millim. Waves* 30 (4), 372–376.

- Maulik, U., Bandyopadhyay, S., 2002. Performance evaluation of some clustering algorithms and validity indices. *IEEE Trans. Pattern Anal. Mach. Intell.* 24 (12), 1650–1654.
- Omkar, S.N., Khandelwal, Rahul, Santhosh, Yathindra, Narayana Naik, G., Gopalakrishnan, S., 2008. Artificial immune system for multi-objective design optimization of composite structures. *Eng. Appl. Artif. Intell.* 21 (8), 1416–1429.
- Rignot, E.J.M., Van Zyl, J.J., 1993. Change detection techniques for ERS-1 SAR data. *IEEE Trans. Geosci. Remote Sens.* 31 (4), 896–906.
- Rosenfield, G.H., Fitzpatrick-Lins, A., 1986. A coefficient of agreement as a measure of thematic classification accuracy. *Photogramm. Eng. Remote Sens.* 52 (2), 223–227.
- Schaffer, J.D., 1985. Multiple-objective optimization with vector evaluated genetic algorithms. In: *Proceedings of the First International Conference on Genetic Algorithms, Genetic Algorithms and their Applications*. Lawrence Erlbaum, pp. 93–100.
- Shang, R.H., Jiao, L.C., Liu, F., 2012. A novel immune clonal algorithm for MO problems. *IEEE Trans. Evol. Comput.* 16 (1), 35–50.
- Timmis, J., Neal, M., Hunt, J., 1999. Data analysis with artificial immune systems and cluster analysis and kohonen networks: some comparisons. In: *Proceeding of the International Conference Systems and Man and Cybernetics*, pp. 922–927.
- Wan, H.L., Jiao, L.C., 2011. Change detection in SAR images by means of grouping connected regions using clone selection algorithm. *Electron. Lett.* 47 (5), 338–339.
- Yang, D.D., Jiao, L.C., Gong, M.G., 2011. Artificial immune multi-objective SAR image segmentation with fused complementary features. *Inf. Sci.* 181 (13), 2797–2812.
- Yang, D.D., Jiao, L.C., Niu, R.C., Gong, M.G., 2014. Investigation of combinational clustering indices in artificial immune multi-objective clustering. *Comput. Intell.* 30 (1), 115–144.
- Yoo, J., Hajela, P., 1999. Immune network simulations in multicriterion design. *Struct. Multidiscip. Optim.* 18 (2–3), 85–94.
- Zhang, X.H., Chen, J.W., Meng, H.Y., 2013. A novel SAR image change detection based on graph-cut and generalized Gaussian model. *IEEE Trans. Geosci. Remote Sens. Lett.* 10 (1), 14–18.
- Zou, F., Wang, L., Hei, X.H., Chen, D.B., Wang, B., 2013. Multi-objective optimization using teaching-learning-based optimization algorithm. *Eng. Appl. Artif. Intell.* 26 (4), 1291–1300.